Proceedings of the 9ICEG
9th International Congress on Environmental Geotechnics
25-28 June, 2023 | Chania, Greece
© Authors: All rights reserved, 2023
https://doi.org/10.53243/ICEG2023-441

Optimization and propagation of uncertainties of a THM numerical model representing a nuclear waste repository concept

M. Wojnarowicz[1], A. Madaschi[2] and L. Laloui[3]

[1]*Ph.D. student, Soil Mechanics Laboratory, Ecole Polytechnique Fédérale de Lausanne, CH-1015 Lausanne, Switzerland,*

email: matthias.wojnarowicz@epfl.ch

[2]*Dr., Nesol – Numerical Engineering Solutions Sàrl, CH-1024 Ecublens, Switzerland,*

email: aldo.madaschi@nesol.net

[3]*Professor, Soil Mechanics Laboratory, Ecole Polytechnique Fédérale de Lausanne, CH-1015 Lausanne, Switzerland,*

email: lyesse.laloui@epfl.ch

ABSTRACT

Nuclear waste repositories are being considered by many countries to be the best solution to deal with the increasing amount of High-Level Waste (HLW) from nuclear power plant operation and decommissioning. The Swiss repository concept has been assessed since the '90s in Mont Terri Underground Rock Laboratory (URL) via numerous in-situ experiments. Among the different experimentations taking place in the URL, the Full-scale Emplacement (FE) is an in-situ experiment that mimics the construction, backfilling, and early-stage evolution of the repository tunnel. Close and far fields have been extensively instrumented to identify the main repository-induced effects (RIE) associated with the excavation and waste decaying. In this framework, modeling the FE experiment is extremely valuable to scope the main parameters acting on the RIE in a relatively small timeframe. In the present research, we use the FE experiment database to validate a coupled Thermo-Hydro-Mechanical (THM) finite element model of the problem and quantify the inherent uncertainties. To do so, we first performed a sensitivity analysis on the parameter domain to identify the parameters prone to be optimized using a variance-based strategy. Once the main parameters influencing the THM behavior were identified, a Bayesian inference approach was adopted to estimate the modeling uncertainty by comparing the numerical results to the experimental monitoring data. Results showed good agreement with the experimental data for temperature and pore-pressure close field sensors with relatively small model variance and showed the applicability of such a modeling approach for RIE assessment.

Keywords: Nuclear waste, Geological repository, thermo-hydro-mechanical analysis, Finite Element Method, Model calibration, Uncertainty quantification

1 INTRODUCTION

Over the past century, nuclear waste production is on constant growth with no effective solution to dispose of them. In this context, nuclear waste repositories appear as a potential permanent relief solution and are thus assessed by most countries around the world. It generally consists of a network of galleries located in a suitable rock host formation where the nuclear packages are disposed of (Garitte et al., 2013). In Switzerland, post-closure safety is ensured by the multibarrier system consisting of several barriers acting together to prevent radioactive leakage. This multibarrier system is composed of the canister (containing the vitrified spent fuel), an engineered bentonite-based backfill material (GBM), and the geological formation itself, the Opalinus Clay (OPA) (Leupin et al., 2016). In such a structure, Thermo-Hydro-Mechanical (THM) processes are highly coupled, and numerous interactions are expected to occur.

One of the main concerns relative to nuclear waste emplacement is the heat emitted by the nuclear packages decaying, which could impair the different barriers. In this framework, modeling tools are

extremely valuable for locating potential safety hazards and testing different configurations. However, the complex geometry, high number of THM coupling, and the problem non-linearities can make the modeling challenging. Moreover, the determination of the parameters involved in the parametrization leads to significant uncertainties propagations that have to be quantified to use the model in the context of safety verification processes.

In Mont Terri URL, different experiments have already been subjected to scoping exercises on specific parts of the multi-barrier system but very few on the global full-scale experiment. As an example, the HE-D heater experiment was designed to characterize the behavior of the OPA with respect to high temperatures (Bossart et al., 2017). This experiment led to the classification of the intensity of cross-coupling between the THM processes (Garitte et al., 2017). It has shown that the largest displacement contribution can be attributed to the thermal expansion and pore pressure dissipation, implying a strong coupling from thermal to mechanical and hydraulic behavior (Gens et al., 2017). The heat transport appears to be mainly driven by conduction which tends to indicate that the coupling from thermal to hydraulic is low. Similarly, no significant porosity variation was observed able to impact the thermal conductivity of the medium, and the size of the Excavated Damaged Zone (EDZ) does seem to be affected by temperature variation (Gens et al., 2017). The HE-E experiment aimed to study the re-saturation of the zone around the tunnel, and its impact on the THM evolution was also extensively studied in Mont Terri (Wieczorek et al., 2017). As for the HE-D experiment, the HE-E experiment has been the subject of modeling exercises (Garitte et al., 2017; Gaus et al., 2014). It has shown a significant dependency of the initial conditions to the outputs, which indicates that the excavation/ventilation has to be explicitly modeled to have comparable results. Moreover, the exercise confirmed a correct implementation of the different boundary conditions and retention models. Finally, the FE experiment represents the last addition to the Mont Terri URL that is currently ongoing and is the focus of the present research.

Sensitivity analyses are an effective way to understand the main driving physical processes and are often used to identify which parameters are prone to be optimized in priority. However, classical sensitivity analyses are time-consuming, and the interpretations are not straightforward when many parameters have to be tested. In this framework, Sobol's sensitivity analysis can be used. This type of sensitivity analysis uses the variance decomposition of the model output into fractions of each individual or group of parameters over the total variance (Sobol, 2001). This strategy gives an easy-to-understand measure of the effect of an input on a specific output via sensitivity indexes.

The calibration of a model consists of an iterative procedure that evaluates an objective function leading to a better representation of the output of a model with respect to measured data. Often, this function is the square of the difference between the model outputs and the data (Levasseur, 2007). In the present research, a Bayesian approach was adopted where the objective function consists of maximizing the posterior probability by assuming a classical normal distribution describing the observation (Sivia & Skilling, 2006).

2 IMPLEMENTATION IN A NUMERICAL CODE

The implementation of the numerical model was conducted on the Finite Element numerical code, Code_Aster (EDF, 1989). A simplified cross-section of the FE tunnel, perpendicular to the tunnel axis was used. The geometry of the experiment was idealized as shown in Figure 1. The tunnel is made of a circular excavation, a concentric Excavated Damaged Zone (EDZ), a shotcrete lining, the backfilled Granular Bentonite Material (GBM), and the heater (Figure 1b). The initial and boundary conditions were determined from a survey done by Bossart & Wermeille (2013) as well as the early results of the FE monitoring. The boundary and initial conditions are thus in equilibrium with the lithostatic state of the region. Previous scoping calculation exercises have shown non-negligible perturbations in the initial field that could impact the modeling results (Garitte et al., 2017; Gaus et al., 2014). Therefore, the construction and emplacement of the different elements of the experiment were explicitly modeled. Similarly, the OPA anisotropy was modeled with a bedding plane dipping 35° southeast. Moreover, the desaturation induced by the ventilation of the tunnel during its construction was modeled with a capillary pressure prescribed at the tunnel excavated face and lining. Following the real experiment schedule, the overall experiment construction was assumed to last 1'553 days, followed by the heating phase.

The mediums are assumed to be poroelastic, and the pores are occupied by two constituents, coexisting in the two phases for the water (e.g., liquid water and vapor) and the Bishop's (1963) effective stress theory is assumed. The heat follows Fourier's conductive law (1822), and the transports of the mobile

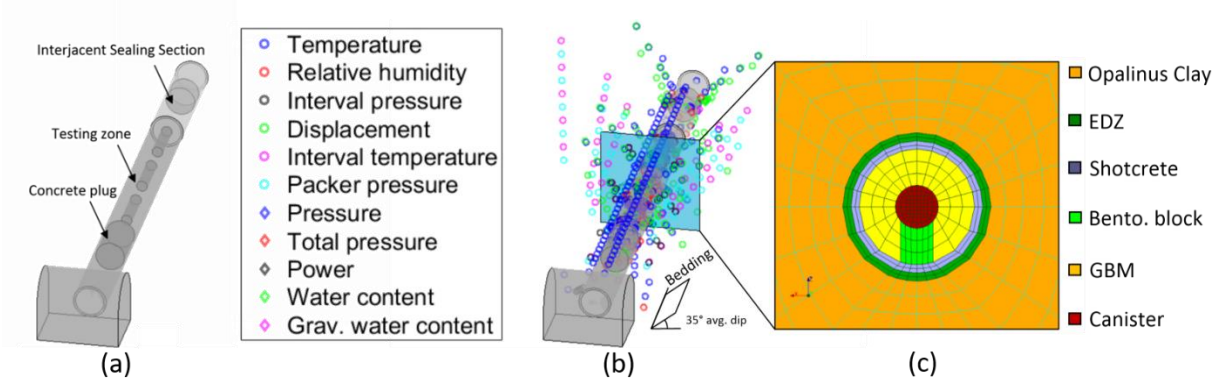


Figure 1. *(a) Geometry of the experiment, (b) Monitoring of the FE experiment and (c) simplified model.*

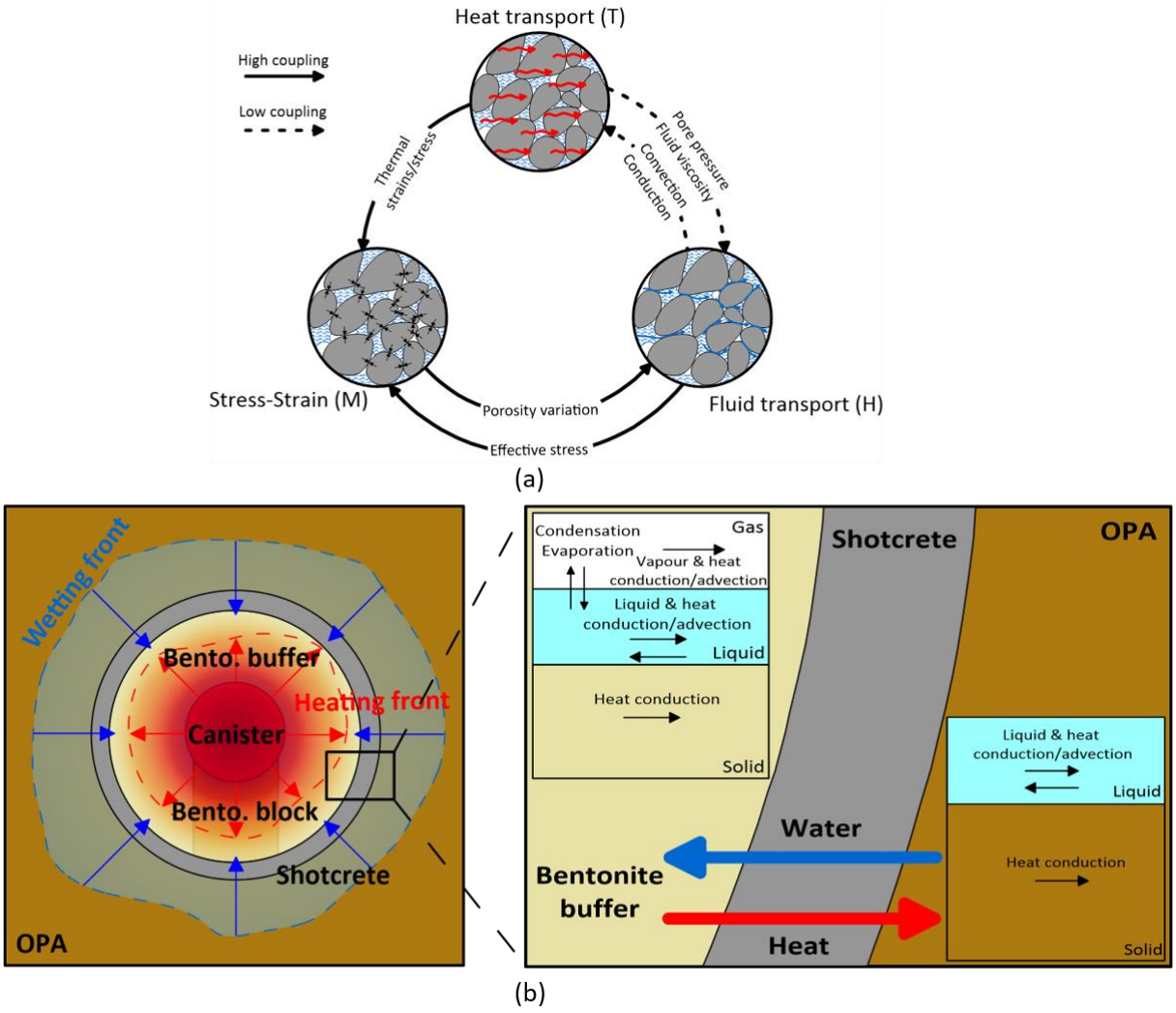


Figure 2. *(a) THM interaction of the numerical model and (b) expected heat and hydraulic transfer.*

phases are described by the classical Darcy's (1856) for the advection and Fick's (1855) laws for the diffusion. The resulting model consists of solving the different conservation equations (i.e. mass, energy and momentum balance equations). Further equilibrium equations are needed to close the problem as a retention model to link the pore pressures to the saturation and an air/vapor pressures relationship. In the present research, the Van Genuchten-Mualem model (Mualem, 1976; van Genuchten, 1980) was

used for the retention model, and Dalton's law was adopted for describing the partial pressure of the two-gas constituent. The THM model is highly coupled; a summary can be found in Figure 2a.

3 VARIANCE-BASED SENSITIVITY ANALYSIS

Sensitivity analysis is an effective way to assess how complex interaction evolves with respect to parameterization. In the present document, we focus on Sobol's sensitivity analysis. It should be noted that we restrict ourselves to the computation of the first, second, and total-order indexes. It yields:

$$S_i = \frac{V_i}{V(Y)} \quad (1)$$

$$\boldsymbol{S_{ij|i\neq j} = \frac{V_{ij}}{V(Y)}} \quad (2)$$

$$S_{Ti} = S_i + \sum S_{ij} + \sum S_{ij\ldots n} \quad (3)$$

S_i measures the partial variance of a single parameter i over the total variance. Similarly, $S_{ij|i\neq j}$ is the partial variance of the pair *ij* over the total variance and measures the combined effect of the parameters ij. Finally, the total effect index S_T is the sum of the parameter's first and higher-order interactions. To compute these sensitivity indexes, one can use the Monte Carlo estimator (Saltelli et al., 2010). The Python open-source library SALIB (Herman & Usher, 2017; Iwanaga et al., 2022) was used to generate the input samples. The complete methodology for the sensitivity indexes computation was developed by Saltelli et al., 2008. Without prior knowledge of the parameter's distributions, one can fit a classical normal distribution using the "3-sigma rule" and the bounds found in the literature (maximum and minimum bounds corresponding to a 0.3% probability of occurrence; see Table 1).

Table 1. *Parameters range and distribution (Bossart, 2011; Crisci, 2019; Fernàndez-Garcia et al., 2007; Ferrari et al., 2014; Gaus, et al., 2014; Gens et al., 2011; H. Bock, 2009; Jobmann & Polster, 2007; Marschall et al., 2004; Mayor et al., 2007; Mügler et al., 2006; Muñoz et al., 2009; Tang & Cui, 2010; M. Villar & Gomez-Espina, 2008; M. V. Villar & Romero, 2020; Wieczorek et al., 2011; Wileveau, 2005)***.**

Parameter	Unit	Min	Max	μ	σ^2
$\lambda_{S,bpel}$	W/(mK)	7.00E-01	1.50E+00	1.10E+00	1.33E-01
$\lambda_{D,bpel}$	W/(mK)	2.00E-01	5.00E-01	3.50E-01	1.50E-02
Cp_{bpel}	J/(kgK)	8.00E+02	1.00E+03	9.00E+02	3.33E+01
$\lambda_{S,shcr}$	W/(mK)	1.40E+00	2.00E+00	1.70E+00	1.00E-01
$\lambda_{D,shcr}$	W/(mK)	5.00E-01	1.00E+00	7.50E-01	8.33E-02
Cp_{shcr}	J/(kgK)	6.50E+02	8.50E+02	7.50E+02	3.33E+01
$\lambda_{//,opa}$	W/(mK)	1.70E+00	2.70E+00	2.20E+00	1.67E-01
$\lambda_{\perp,opa}$	W/(mK)	8.00E-01	2.60E+00	1.70E+00	3.00E-01
Cp_{opa}	J/(kgK)	7.50E+02	1.20E+03	9.75E+02	7.50E+01
n_{bpel}	-	1.70E+00	2.40E+00	2.05E+00	1.17E-01
P_{bpel}	Pa	5.00E+06	7.00E+07	3.75E+07	1.08E+07
k_{bpel}	m²	1.00E-20	5.00E-20	3.00E-20	6.67E-21
n_{shcr}	-	1.20E+00	1.80E+00	1.50E+00	1.00E-01
P_{shcr}	Pa	1.00E+06	1.00E+07	5.50E+06	1.50E+06
k_{shcr}	m²	1.00E-18	1.00E-17	5.50E-18	1.50E-18
k_{edz}	m²	1.00E-21	6.00E-20	3.05E-20	9.83E-21
n_{opa}	-	1.30E+00	2.20E+00	1.75E+00	1.50E-01
P_{opa}	Pa	4.00E+06	8.00E+07	4.20E+07	1.27E+07
$k_{//,opa}$	m²	9.00E-21	6.00E-20	3.45E-20	8.50E-21

$k_{\perp,opa}$	m²	6.00E-21	6.00E-20	3.30E-20	9.00E-21

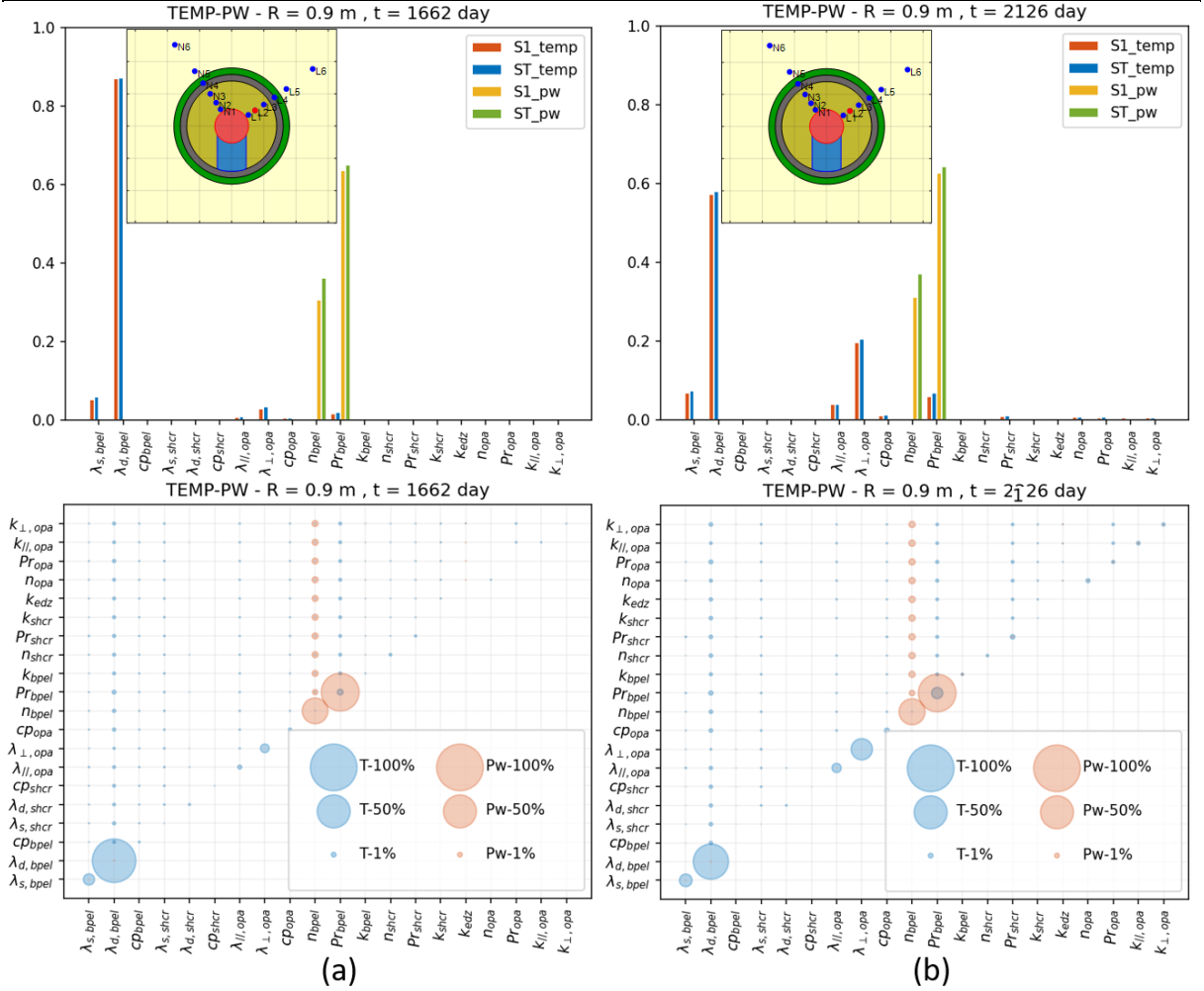


Figure 3. *(a) Sensitivity analysis at a control point located in the GBM after 109 days of heating. (b) Sensitivity analysis at a control point located in the GBM after 573 days of heating (top: first and total index; bot: first and second order index).*

The strategy adopted in this document is to scope specific locations close to real sensor positions in the OPA and GBM to capture the effect of each parameter on specific outputs through time. Here we focused on two outputs, the temperature and the pore pressure and two control times are 1662 and 2126 days (i.e. after 109 and 573 days of heating). For conciseness, we only displayed the main outcomes of the sensitivity analysis in the direction parallel to the bedding since the anisotropy is mirroring the results in the other direction.

Figure 3 and Figure 4, show an example of sensitivity analysis performed in this study. The top figures represent the main and total order Sobol's indexes for two sensors with respect to the different parameters tested and the bot figures the interaction between every two sets of parameters. From Figure 3a, one can identify that the highest contributors to the temperature in the GBM are the GBM thermal conductivities at the early stage. This then decreases with respect to the OPA conductivities (Figure 3b). This can easily be explained by the heating front reaching the OPA and acting as a heat sink which then influences the GBM temperature. Similarly, the conductivity perpendicular to the bedding plan is the main contributor to the temperature through time for the control point present in the OPA (Figure 4). One may observe that the heat transfer is mainly conductive the hydraulic parameters having a small influence on the temperature. Moreover, we can observe from the top figures close values between S_i and S_T. This indicates low interactions between the different factors. This low interaction is confirmed with both bottom figures showing every two parameter sets interactions S_{ij} above the diagonal and the first-order index S_i on the diagonal.

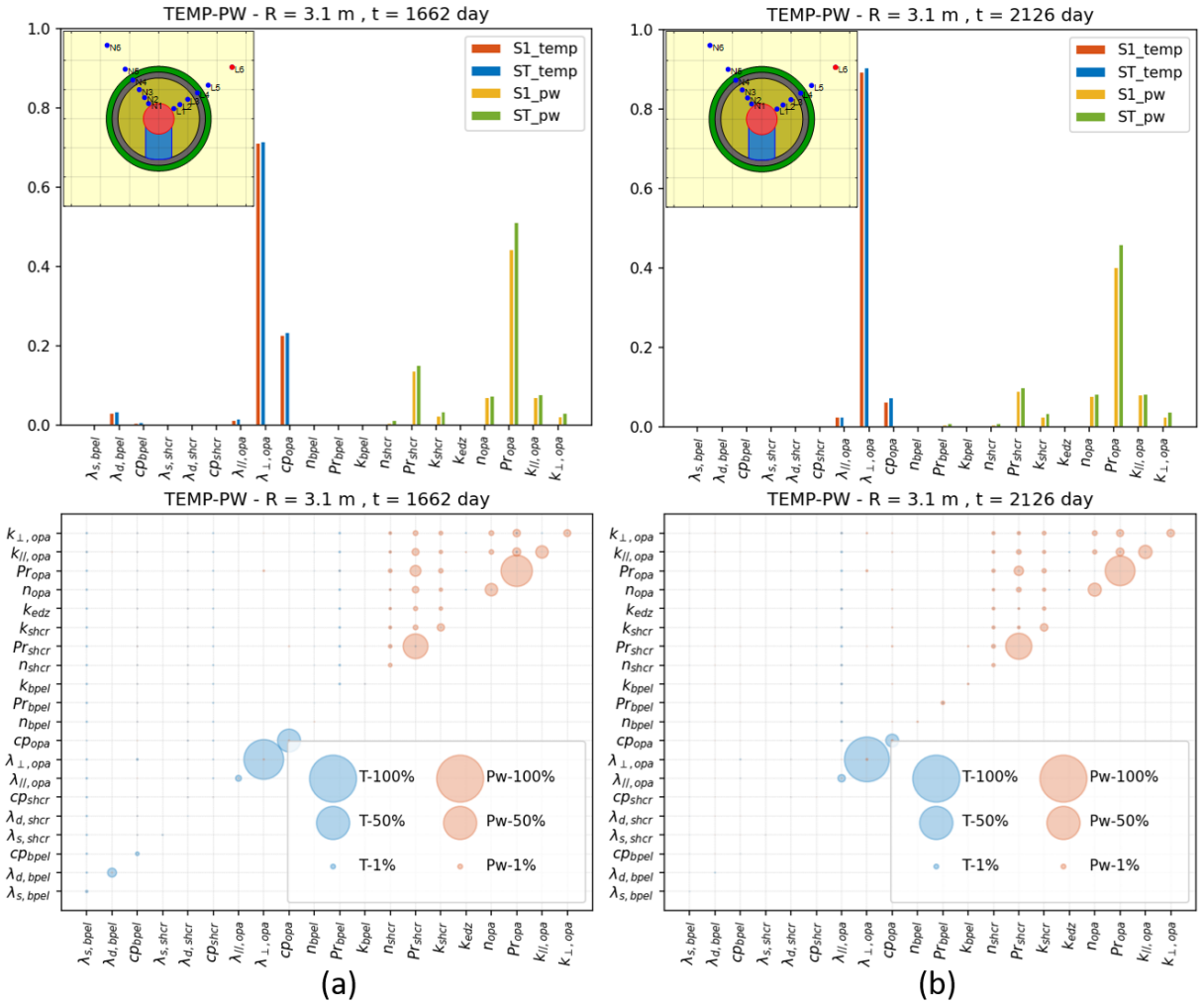


Figure 4. *(a) Sensitivity analysis at a control point located in the OPA after 109 days of heating. (b) Sensitivity analysis at a control point located in the OPA after 573 days of heating (top: first and total index; bot: first and second order index).*

Similarly, one can observe an influence of the permeabilities, shape parameters, and air entry pressure of the Van Genuchten water retention curves on the pore pressure. Furthermore, Figure 4 shows that the shotcrete air entry pressure also has a significant role in the pore pressure development in the OPA. Indeed, it may control the re-saturation of the GBM by enabling or disabling the water flow through it. As a first approximation, we choose to keep its value as it is to focus on the OPA parametrization. Moreover, one can observe a small interaction between the shotcrete and OPA parameters (Figure 4 bottom). Those interaction remains relatively small and can thus be neglected.

Note that, a similar analysis was done on the control points located perpendicular to the anisotropy orientation and showed mirrored results, indicating that the intrinsic permeabilities and thermal conductivities should be optimized together to capture the entire RIE evolution. It also shows that the thermal and hydraulic parts are only weakly coupled and can thus be uncoupled as a first approximation, reducing the number of factors in our calibration.

4 BAYESIAN INFERENCE METHOD

The Bayesian inference method is based on the well-known Bayes theorem. It describes an event probability, knowing a conditional probability related to this event. Only the fundamentals of the method, important to understand the approach, are developed here for conciseness; more details can be found in Sivia & Skilling, 2006.

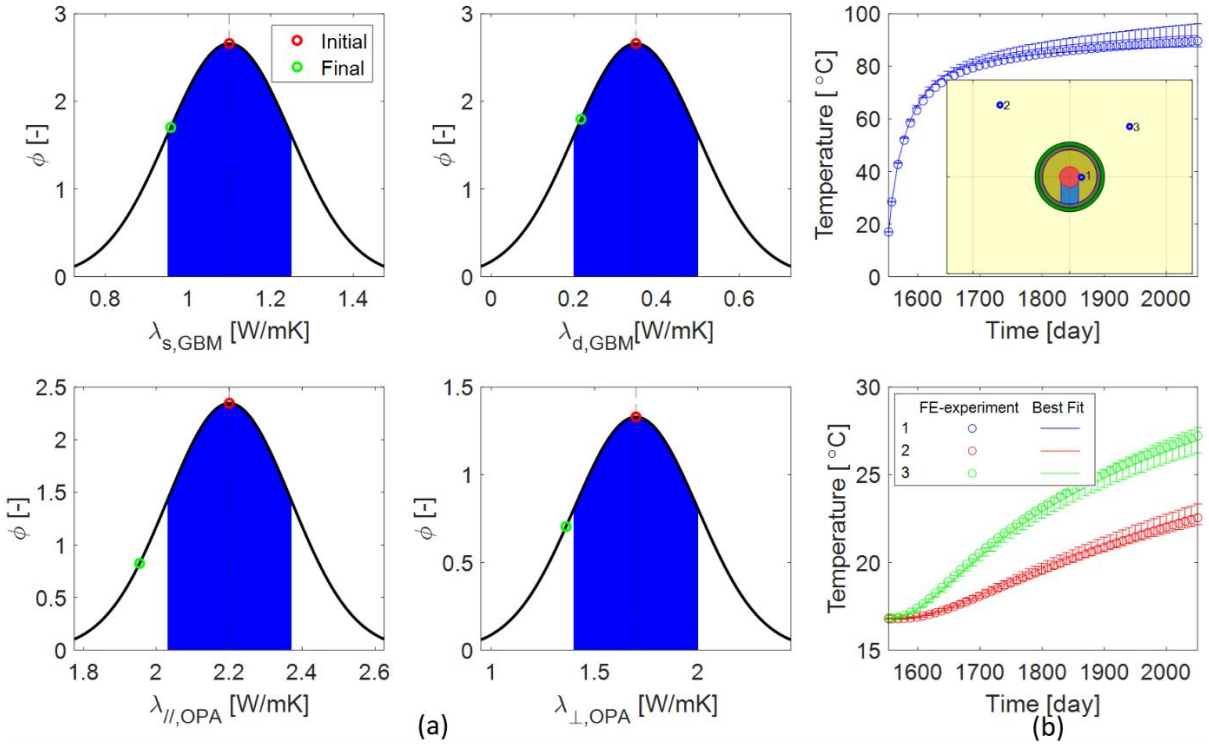


Figure 5. *Temperature calibration and uncertainty propagation. (a) A priori density function of the thermal factors and (b) results on three temperature sensors.*

The Bayes theorem yields:

$$\overbrace{p(hypothesis|data)}^{posterior} = \frac{\overbrace{p(data|hypothesis)}^{likelihood}\overbrace{p(hypothesis)}^{prior}}{\underbrace{p(data)}_{evidence}} \quad (4)$$

Let's note in the next equations A for the data and B for the hypothesis. The probability $p(B|A)$ is thus the conditional posterior probability of B given A. $p(A|B)$, refers to the likelihood function and defines the conditional probability of A given B. $p(B)$ defines the a priori probability of our hypothesis. Finally, $p(A)$ represents the evidence. $p(A)$ is thus a normalizing constant and can therefore be neglected. The equation thus yields:

$$p(B|A) \propto p(A|B)p(B) \quad (5)$$

The Bayes theorem can be used as an objective function in any calibration procedure to estimate the parameter uncertainties. To do so, one can maximize the joint posterior probability given the observation. In this framework, we can define the experimental data set of observations $\boldsymbol{y} = \{y_1, y_2, \dots, y_N\}$ and the simulated results $f(\boldsymbol{\theta}, t)$, where $\boldsymbol{\theta}$ is the vector of model parameters. Note that several experiments can be used simultaneously and the resulting objective function is the sum of the individual ones. For each data point, it is possible to define a statistical normal model $N(\boldsymbol{\theta}, \sigma^2)$ similar for each dataset where σ^2 is the model variance with respect to the measured value. The total uncertainty of an experiment is thus represented by the joint probability at each data point as follows:

$$p(\boldsymbol{\theta}|\boldsymbol{y}) \propto \prod_{i=1}^{N} p(\boldsymbol{y_i}|\boldsymbol{\theta})\, \boldsymbol{p}(\boldsymbol{\theta}) \quad (6)$$

When the optimum of this joint probability over each data point is reached, the resulting parameter set noted $\boldsymbol{\theta}^*$ minimizes both the error between the two curves and the inherent variance σ^{2*} of the model. The variance can be interpreted as the model uncertainties and constitute an upper bound to draw 95% confidence bounds around our modeling results. For convenience, we applied a log to the objective function to work with sums rather than products.

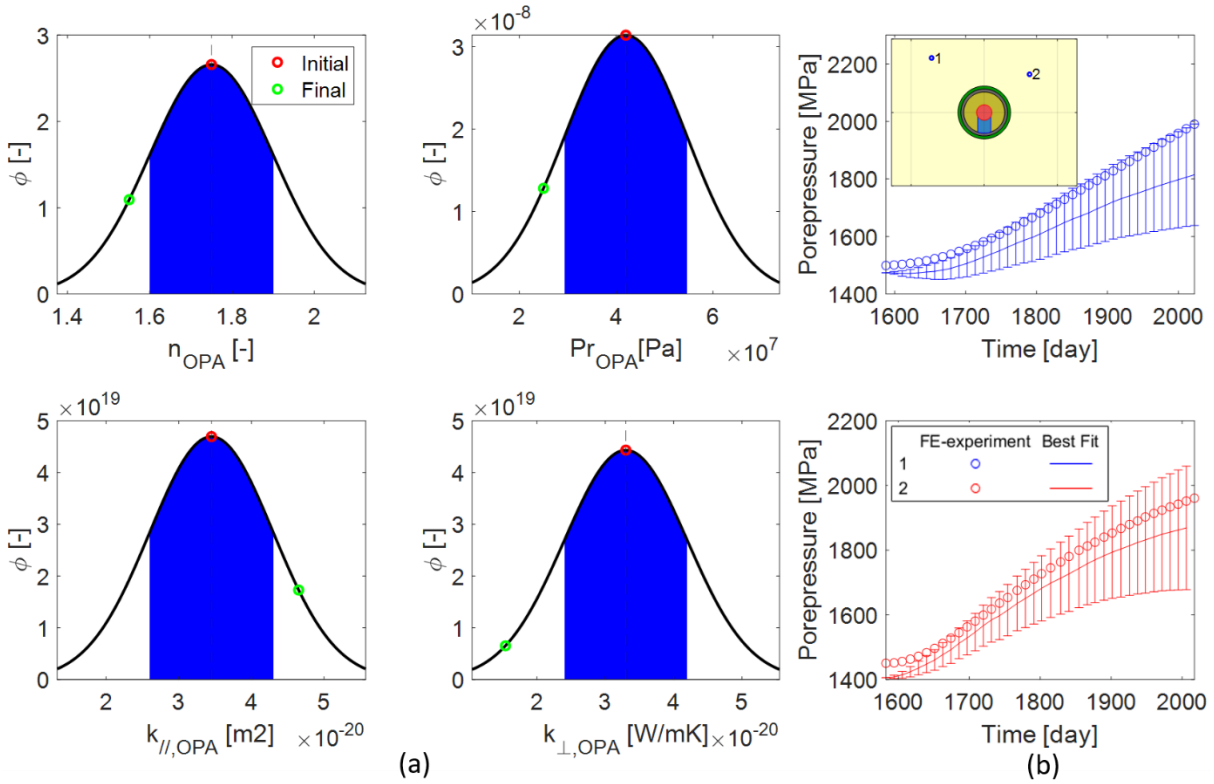


Figure 6. *Pore pressure calibration and uncertainties propagation. (a) A priori density function of the hydraulic factors and (b) results on two pore pressure sensors.*

It yields:

$$log\big(p(\boldsymbol{\theta}|\boldsymbol{y})\big) \propto \sum_{i=1}^{N} log\big(p(y_i|\boldsymbol{\theta})\big) + log(p(\boldsymbol{\theta})) \quad (7)$$

From the sensitivity analysis, we determined that the thermal and hydraulic parts could be uncoupled and we observed that the main influencing parameters on the temperature were the different thermal conductivities. Moreover, we observe that the OPA thermal conductivities have a non-negligible impact on temperature evolution at an early stage in the GBM. Furthermore, we observed that the OPA anisotropy significantly impacts the close field temperature. Therefore, we selected two points sensors in the OPA around the tunnel to capture the anisotropy effect and one in the GBM. The selected factors of interest are thus the dry and saturated conductivities of the GBM and the OPA conductivities in both directions (**Figure 5**a). The resulting global probability for this example can be therefore defined as:

$$log(p(\boldsymbol{\theta}|\boldsymbol{T},\boldsymbol{t})) \propto \sum_{i=1}^{tf} log\big(p(T_1|\boldsymbol{\theta},t_i)\big) + \sum_{i=1}^{tf} log\big(p(T_2|\boldsymbol{\theta},t_i)\big) + \sum_{i=1}^{tf} log\big(p(T_3|\boldsymbol{\theta},t_i)\big) + log(\boldsymbol{p}(\boldsymbol{\theta})) \quad (8)$$

Where T_i represent the calculated temperature for each time t_i at the sensor of interest. The SciPy python library (Virtanen et al., 2020) was used to maximize the objective function and the results can be seen in **Figure 5**b and **Figure 6**b. One may observe that the temperature was well represented and the corresponding uncertainties relatively small (**Figure 5**b). Moreover, the end parameter values lie in, or close to, the first quantile of the normal a priori distribution indicating that our parameter's first estimation was correct.

Similarly, we are interested in optimizing the OPA close field pore pressure. From the sensitivity analysis outcomes, we observed that the OPA Van Genuchten retention curves parameters and its intrinsic permeability are the main contributors to the pore pressure evolution. Those parameters are thus selected to be the factors of interest for this second calibration round. **Figure 6** shows the results of this second analysis. The performed analysis also managed to reproduce the FE measurements. However, higher uncertainties were found for both sensors, which tends to indicate that the selected factors might be insufficient to characterize the pore pressure at those locations. It could thus be beneficial for future analysis to include more factors to the analysis as the shotcrete air entry pressure.

5 CONCLUSION

Model verification/validation and the quantification of their inherent uncertainties are a topic of great interest to both government and industry. The quantification of the confidence and accuracy of a numerical model can provide valuable insights to support strategic decisions for long-term repository safety. This is extremely relevant in the framework of nuclear waste management since it will impact future generations.

The scope of this paper thus consists of the implementation of a stochastic methodology to calibrate and estimate the model uncertainties. The strategy is based on the maximum posterior estimation of the Bayesian probability of the observation. This method was able to define an optimum parameter set of the statistical model while rigorously giving a 95% interval of confidence. The analysis was performed on several selected sensors of an in-situ full-scale experiment which was based on the outcomes of a prior spatiotemporal variance-based sensitivity analysis. The sensitivity analysis successively identified the main influencing parameters acting on the temperature and pore pressure at specific sensor locations. It showed a heat transfer process mainly conductive, allowing the uncoupling of the thermal parts to the hydraulic one. This was used to reduce the number of factors to optimize by only considering conductive the heat transfer coefficients for the heating stage. The temperature was well represented in the experiment's close field which allowed us to pursue the hydraulic behavior optimization. The calibration performed on the OPA permeability and retention parameters showed a good match with the in-situ data. Furthermore, it should be noted that the parameter values after the calibration remained in the a priori interval of confidence defined initially which indicates that the used formulation represents well the reality of interest.

The showed methodology was able to reproduce quite well the experiment while yielding a small variance for the model uncertainties. It shows the applicability of such a modeling approach in the assessment of complex coupled THM behavior providing solid bases for repository safety analysis. At this stage, the strategy could be improved by adding more factors (e.g., shotcrete air entry pressure), considering more sensors across the model, and taking into account the uncertainties coming from the measurements.

6 ACKNOWLEDGEMENTS

We would like to acknowledge NAGRA, the Swiss national cooperative society of radioactive waste storage, for funding this project under the order n° 21’844.

REFERENCES

Bossart, P. (2011). *Characteristics of the Opalinus Clay at Mont Terri*.

Bossart, P., Jaeggi, D., & Nussbaum, C. (2017). Experiments on thermo-hydro-mechanical behaviour of Opalinus Clay at Mont Terri rock laboratory, Switzerland. *Journal of Rock Mechanics and Geotechnical Engineering*, *9*(3), 502–510. doi:10.1016/j.jrmge.2016.11.014

Bossart P., & Wermeille S. (2013). The stress field in the Mont Terri region. Data compilation. In P. Heitzmann & J.-P. Tripet (Eds.), *Mont Terri Project – Geology, Paleohydrology and Stress Field of the Mont Terri Region* (pp. 65–92).

Crisci, E. (2019). Hydro-mechanical response of Opalinus Clay shale: dependency on composition and burial depth, 207. Retrieved from http://infoscience.epfl.ch/record/271680

Electricité de France. (1989). Finite element Code_Aster, Analysis of Structures and Thermomechanics for Studies and Research. Open source on www.code-aster.org.

Fernàndez-Garcia, D., Jaime Gómez-Hernández, J., & Mayor, J.-C. (2007). Estimating hydraulic conductivity of the Opalinus Clay at the regional scale: Combined effect of desaturation and EDZ. *Physics and Chemistry of the Earth*, *32*(8–14), 639–645.

Ferrari, A., Favero, V., Marschall, P., & Laloui, L. (2014). Experimental analysis of the water retention behaviour of shales. *International Journal of Rock Mechanics and Mining Sciences*, *72*, 61–70–61–70.

Garitte, Benoit, Müller, H. R., Vogt, T., Vietor, T., Thatcher, K., & Senger, R. (2013). *Scoping Computations for the Full Scale Emplacement (FE) Experiment in the Mont Terri Underground Rock Laboratory*.

Garitte, B., Nguyen, T. S., Barnichon, J. D., Graupner, B. J., Lee, C., Maekawa, K., … Shao, H. (2017). Modelling the Mont Terri HE-D experiment for the Thermal–Hydraulic–Mechanical response of a bedded argillaceous formation to heating. *Environmental Earth Sciences*, *76*(9). doi:10.1007/s12665-017-6662-1

Garitte, B., Shao, H., Wang, X. R., Nguyen, T. S., Li, Z., Rutqvist, J., … Barnichon, J. D. (2017). Evaluation of the predictive capability of coupled thermo-hydro-mechanical models for a heated bentonite/clay system (HE-E) in the Mont Terri Rock Laboratory. *Environmental Earth Sciences*, *76*(2). doi:10.1007/s12665-016-6367-x

Gaus, I., Garitte, B., Senger, R., Gens, A., Vasconcelos, R., Garcia-Sineriz, J. L., … others. (2014). The HE-E experiment: lay-out, interpretation and THM modelling. *Nagra Arbeitsbericht NAB*, 14–53–14–53.

Gaus, I., Wieczorek, K., Schuster, K., Garitte, B., Senger, R., Vasconcelos, R., & Mayor, J. C. (2014). EBS behaviour immediately after repository closure in a clay host rock: HE-E experiment (Mont Terri URL). *Geological Society Special Publication*, *400*(1), 71–91. doi:10.1144/SP400.11

Gens, A., Vaunat, J., Garitte, B., & Wileveau, Y. (2011). *In situ behaviour of a stiff layered clay subject to thermal loading: observations and interpretation*. In *Stiff Sedimentary Clays: Genesis and Engineering Behaviour: Géotechnique Symposium in Print 2007* (pp. 123–144–123–144).

Gens, A., Wieczorek, K., Gaus, I., Garitte, B., Mayor, J. C., Schuster, K., … Trick, T. (2017). Performance of the Opalinus Clay under thermal loading: experimental results from Mont Terri rock laboratory (Switzerland). *Swiss Journal of Geosciences*, *110*(1), 269–286–269–286. Retrieved from https://doi.org/10.1007/s00015-016-0258-8

H. Bock. (2009). *RA Experiment: Updated review of the rock mechanics properties of the Opalinus clay of the Mont Terri URL based on laboratory and field testing*.

Herman, J., & Usher, W. (2017). SALib: An open-source Python library for Sensitivity Analysis. *The Journal of Open Source Software*, *2*(9), 97. doi:10.21105/joss.00097

Iwanaga, T., Usher, W., & Herman, J. (2022). Toward SALib 2.0: Advancing the accessibility and interpretability of global sensitivity analyses. *Socio-Environmental Systems Modelling*, *4*, 18155. doi:10.18174/sesmo.18155

Jobmann, M., & Polster, M. (2007). The response of Opalinus clay due to heating: A combined analysis of in situ measurements, laboratory investigations and numerical calculations. *Physics and Chemistry of the Earth, Parts A/B/C*, *32*(8), 929–936. Retrieved from https://www.sciencedirect.com/science/article/pii/S1474706506002555

Leupin, O. X., Smith, P., Marschall, P., Johnson, L., Savage, D., Cloet, V., … Senger, R. (2016). *High-level waste repository-induced effects*. Retrieved from www.nagra.ch

Levasseur, S. (2007). *Analyse Inverse en Géotechnique: développement d'une méthode à base d'algorithmes génétiques.* Retrieved from https://tel.archives-ouvertes.fr/tel-00185671

Marschall, P., Croisé, J., Schlickenrieder, L., Boisson, J. Y., Vogel, P., & Yamamoto, S. (2004). Synthesis of hydrogeological investigations at the Mont Terri site (phases 1 to 5). *Mont Terri Project–Hydrogeological Synthesis, Osmotic Flow, Edited by: Heitzmann, P., Reports of the Federal Office for Water and Geology, Geology Series*, *6*, 7–92–97–92.

Mayor, J.-C., Velasco, M., & García-Siñeriz, J.-L. (2007). Ventilation experiment in the Mont Terri underground laboratory. *Physics and Chemistry of the Earth, Parts A/B/C*, *32*(8–14), 616–628–616–628.

Mügler, C., Filippi, M., Montarnal, P., Martinez, J.-M., & Wileveau, Y. (2006). Determination of the thermal conductivity of opalinus clay via simulations of experiments performed at the Mont Terri underground laboratory. *Journal of Applied Geophysics*, *58*(2), 112–129–112–129.

Muñoz, J., Alonso, E. E., & Lloret, A. (2009). Thermo-hydraulic characterisation of soft rock by means of heating pulse tests. *Géotechnique*, *59*(4), 293–306–293–306.

Saltelli, Andrea, Annoni, P., Azzini, I., Campolongo, F., Ratto, M., & Tarantola, S. (2010). Variance based sensitivity analysis of model output. Design and estimator for the total sensitivity index. *Computer Physics Communications*, *181*(2), 259–270. doi:10.1016/j.cpc.2009.09.018

Saltelli, A., Ratto, M., Andres, T., Campolongo, F., Gariboni, J., Gatelli, D., … Tarantola, S. (2008). *Global Sensitivity Analysis. The Primer*. Retrieved from http://www.andreasaltelli.eu/file/repository/A_Saltelli_Marco_Ratto_Terry_Andres_Francesca_Campolongo_Jessica_Cariboni_Debora_Gatelli_Michaela_Saisana_Stefano_Tarantola_Global_Sensitivity_Analysis_The_Primer_Wiley_Interscience_2008_.pdf

Sivia, D. S., & Skilling, J. (2006). *Data Analysis*. Retrieved from http://aprsa.villanova.edu/files/sivia.pdf

Sobol′, I. M. (2001). Global sensitivity indices for nonlinear mathematical models and their Monte Carlo estimates. *Mathematics and Computers in Simulation*, *55*(1–3), 271–280. doi:10.1016/S0378-4754(00)00270-6

Tang, A. M., & Cui, Y. J. (2010). Effects of mineralogy on thermo-hydro-mechanical parameters of MX80 bentonite. *Journal of Rock Mechanics and Geotechnical Engineering*, *2*(1), 91–96. Retrieved from https://www.sciencedirect.com/science/article/pii/S167477551530024X

Villar, M., & Gomez-Espina, R. (2008). Effect of temperature on the water retention capacity of FEBEX and MX-80 bentonites, Unsaturated Soils. *Advances in Geo-Engineering, London, UK*.

Villar, M. V., & Romero, F. J. (2020). Water Retention Curves of Opalinus Clay.

Virtanen, P., Gommers, R., Oliphant, T. E., Haberland, M., Reddy, T., Cournapeau, D., … Vázquez-Baeza, Y. (2020). SciPy 1.0: fundamental algorithms for scientific computing in Python. *Nature Methods*, *17*(3), 261–272. doi:10.1038/s41592-019-0686-2

Wieczorek, K., Gaus, I., Mayor, J. C., Schuster, K., García-Siñeriz, J. L., & Sakaki, T. (2017). In-situ experiments on bentonite-based buffer and sealing materials at the Mont Terri rock laboratory (Switzerland). *Swiss Journal of Geosciences*, *110*(1), 253–268. doi:10.1007/s00015-016-0247-y

Wieczorek, K., Miehe, R., & Garitte, B. (2011). Measurement of thermal parameters of the HE-E buffer materials. *EURATOM Project PEBS Deliverable D*, *2*, 2–5–2–5.

Wileveau, Y. (2005). THM behaviour of host rock: (HE-D experiment): Progress Report September 2003 – October 2004. *TECHNICAL REPORT TR 2005-03 August 2005*.